



Cite this: *Photochem. Photobiol. Sci.*, 2017, **16**, 1252

Spectral and photochemical properties of hybrid organic–inorganic nanosystems based on CdS quantum dots and merocyanine ligands†

Oleg V. Chashchikhin * and Mikhail F. Budyka 

The spectral and photochemical properties of hybrid organic–inorganic nanosystems (HNSs) were investigated. HNS consisted of CdS quantum dots (QDs) functionalized with ligands containing the isothiouronium anchor group linked by a polymethylene chain with photochromic merocyanine (MC). The HNS synthesis was carried out via a microwave-assisted one-pot technique. Energy transfer from the QDs to MC in the HNS was observed and resulted in QD fluorescence quenching and MC sensitization. Compared to the free MC, *trans*–*cis* photoisomerization of MC in the HNS was suppressed and its photodestruction was accelerated. In addition, upon HNS photolysis by visible light with energy higher than the threshold, the photosensitized destruction of the QDs (which did not absorb the applied light) occurred. The observed effects were proposed to be caused by MC adsorption on QDs surface, which leads to the restriction of the MC photoisomerization and population of the surface electron trap states of the QDs.

Received 7th April 2017,
Accepted 30th May 2017
DOI: 10.1039/c7pp00137a
rsc.li/pps

Introduction

Hybrid organic–inorganic nanosystems (HNS) consisting of inorganic nanoparticles modified with organic ligands are of great interest for various applications.^{1–5} Nanoparticles, in particular, may be colloidal semiconductor quantum dots (QDs). Essentially, almost any colloidal QD is a hybrid system since it contains the shell of an organic stabilizing ligand. However, HNSs usually imply the presence of some “functional” ligands (FLs), which should be able to respond to external impact.

HNSs combine the properties of inorganic (QDs) and organic (FL) subsystems. In addition, a new property may arise, such as energy or electron transfer between the system's components. By modifying the ligand, one can modulate the electron or/and energy transfer processes, thus managing the properties of the HNS in general.^{1,4–8}

Photoswitchable HNSs are of particular interest since their properties are easily manipulated by light, varying the wavelength, intensity and time of the applied irradiation. Such HNSs are first of all promising for fluorescent microscopy and for data storage or processing systems modeling.^{1,9–15}

The design of HNSs gives rise to an array of challenges, such as the thorough selection of the components with

specific spectral properties (for systems with energy transfer) or redox potentials (for systems with electron transfer), an appropriate anchor for FL attachment to the QD surface and a spacer separating them. Moreover, a decrease in the components' stability after their binding was reported, which was attributed to the electron transfer competing with energy transfer (ET), leading to both FL and QDs degradation.^{9,16,17} Furthermore, the CdS nanoparticles are actively used for the photocatalytic decomposition of organic substances.^{18–20}

Thus, the investigation of QDs and FL interactions upon irradiation of the HNS by light is crucial for revealing the photoinduced processes in the HNSs and consequently for the further design of photoswitchable HNSs with desirable properties.

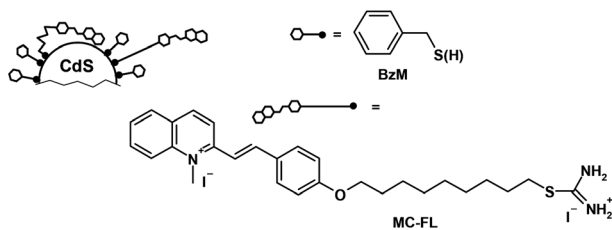
Whilst HNSs consisting of quantum dots and photochromic ligands are well known,^{1,9–15} in our series of studies we first used styrylquinoline ligands, which were shown to be prospective molecular photoswitches.^{21,22} This class of photochromic ligands possess an absorption in the UV spectral range, and thus requires wide band gap semiconductor quantum dots for the HNSs synthesis in order for the spectral properties of both the ligands and quantum dots to be located in the same spectral range. We chose benzyl mercaptan capped CdS quantum dots due to their spectral properties. They possess a quite short-wavelength absorption and a significant Stokes shift (absorption and fluorescence maxima at 333 and 440 nm, respectively).^{23,24}

HNSs are usually obtained by ligand exchange or self-assembly, which are additional procedures after the QD

Institute of Problems of Chemical Physics, Russian Academy of Sciences, pr. Akademika Semenova 1, Chernogolovka, Moscow region, 142432, Russian Federation. E-mail: ovchasch@gmail.com

† Electronic supplementary information (ESI) available: XRD, TEM, SAED, FT-IR. See DOI: 10.1039/c7pp00137a





Scheme 1 A schematic representation of the HNS (the ratio of the sub-systems sizes complies with their real sizes). Two variants of the FL adsorption are shown: the adsorption by the isothiuronium anchor group in the case of the polymethylene chain extended conformation and the adsorption by the MC fragment in the case of the twisted conformation.

synthesis. However, the HNSs investigated in this report were obtained *via* a one-pot, non-injective, microwave assisted technique.^{25,26} We previously reported the spectral and photochemical properties of HNSs containing a styrylquinoline ligand as the FL.²⁷ No energy transfer from the QDs to the FL was observed in the HNSs, their absorption spectra were limited to the UV range, and their photolysis proceeded in two stages – an initial FL *trans-cis* photoisomerization with a high quantum yield (QY) and subsequent QDs photodestruction with a significantly lower QY under prolonged irradiation.

The structure of the photochromic ligand was changed to shift the absorption spectrum of the HNSs to the visible region providing the spectral overlap of the QDs fluorescence and the ligand absorption and creating a prerequisite for the energy transfer from the QDs to the ligands. Herein, we report on the photochemical properties of the two HNSs based on CdS quantum dots and contain different number of FLs (Scheme 1). This FL contains an isothiuronium anchor group, which is linked by the nonamethylene chain to the merocyanine (MC) photochromic fragment capable of undergoing reversible *trans-cis* photoisomerization. The QDs are capped with benzyl mercaptan and have a core diameter of 2.4 nm.

Thus, the spectral and photochemical properties of the QDs and MC ligands look promising for creating photoswitchable HNSs. However, the obtained HNSs containing MC demonstrated very peculiar photochemical properties. Compared to the free MC, the *trans-cis* photoisomerization of MC in the HNS was suppressed and its photodestruction was accelerated. In addition, upon HNS photolysis by visible light with energy higher than the threshold, the photosensitized destruction of the QDs (which did not absorb the applied light) occurred. The observed effects were attributed to the MC adsorption on the QDs surface that led to a restriction of the MC photoisomerization and population of the surface electron trap states of the QDs.

Results and discussion

Spectral properties

The absorption spectra of the investigated HNSs in DMF, as well as the spectra of the constituent subsystems, are shown at

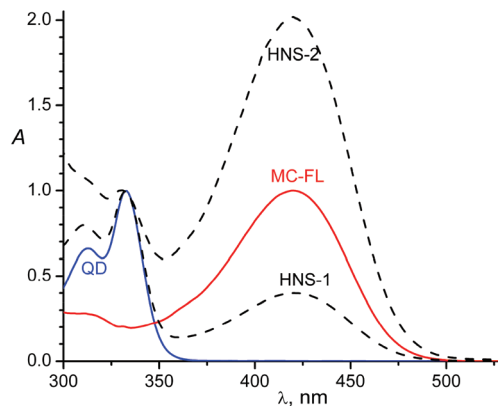


Fig. 1 The normalized absorption spectra of the CdS QDs (diameter of 2.4 nm), HNS-1, HNS-2 and the *trans*-isomer of the functional ligand MC-FL. The QDs and HNSs spectra were normalized at 333 nm and the MC-FL spectrum was normalized at 420 nm.

Fig. 1. Unlinked (“free”) MC-FL and free QD have long-wavelength absorption bands (LWAB) with maxima at 420 nm and 333 nm, respectively. The molar extinction coefficient of the QD is $8 \times 10^4 \text{ M}^{-1} \text{ cm}^{-1}$ at the maximum (333 nm)²⁴ and that of the MC-FL is $3.6 \times 10^4 \text{ M}^{-1} \text{ cm}^{-1}$ for the *trans*-isomer at the maximum (420 nm). The size of the nanoparticles was 2.4 nm.²⁶ Detailed characteristics (TEM, XRD, SAED and IR) of the HNSs, QD and MC-FL have been previously reported²⁶ and can be found in the ESI.†

The spectral properties of HNS-1 and HNS-2 are the superposition of the constituent chromophores – QD and MC. The presence of the MC-FL in the HNSs is clearly corroborated by absorption spectra, where the MC LWAB appears as a separate band (Fig. 1). The electronic absorption spectra were used to calculate the composition of the HNSs (the number of MC-FLs in the HNS, *N*). The average *N* was 1.0 for HNS-1 and 5.6 for HNS-2.^{26,27}

The presence of the two different chromophores in the HNSs was confirmed by photoluminescence (PL) measurements (Fig. 2). Fig. 2a shows the PL emission (1, 2) and excitation (3, 4) spectra of the free QDs (1, excitation at 330 nm; 3, observation at 440 nm) and the MC-FL (2, excitation at 420 nm; 4, observation at 520 nm). The QDs have a PL maximum at 440 nm, whilst the MC-FL has a maximum at 520 nm. The PL excitation spectra reproduced the corresponding absorption spectra.

Analysis of the spectral properties of the QDs and MC-FL shows the spectral overlap of the FL absorption and the QDs PL, which allows the Forster resonance energy transfer (FRET) from the QDs to the FL. Energy transfer was indeed observed in the PL spectra of the HNSs. For instance, the PL emission and excitation spectra of the HNS-1 are shown at Fig. 2b. Two bands corresponding to the QDs (440 nm) and MC (520 nm) were observed in the PL spectrum of HNS-1 upon excitation at the QD absorption maximum (330 nm) (Fig. 2b, spectrum 1). Only one band corresponding to MC was observed upon excitation at the MC-FL absorption maximum (420 nm), where



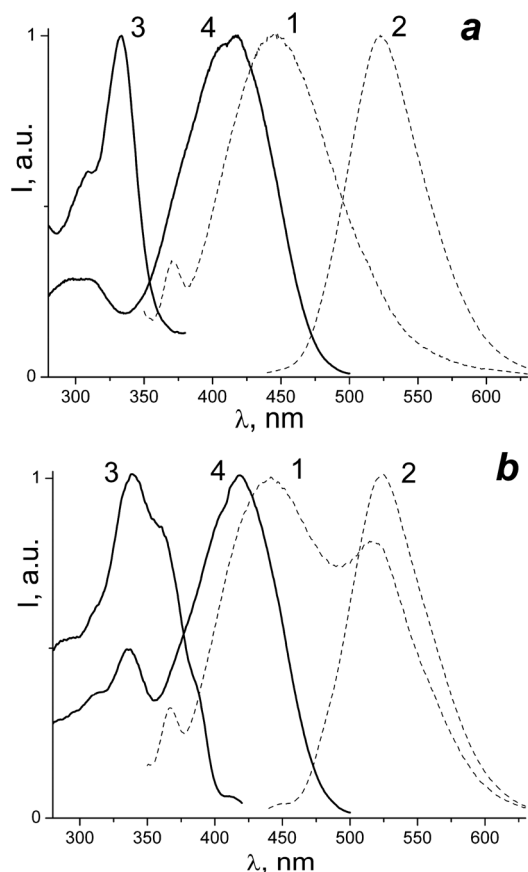


Fig. 2 (a) The photoluminescence spectra: 1 – QDs (excitation at 330 nm) and 2 – MC-FL (excitation at 420 nm); the photoluminescence excitation spectra: 3 – QDs (observation at 440 nm) and 4 – MC-FL (observation at 520 nm); (b) the photoluminescence spectra of HNS-1: 1 – excitation at 330 nm and 2 – excitation at 420 nm; the photoluminescence excitation spectra of HNS-1: 3 – observation at 440 nm and 4 – observation at 520 nm; the spectra are normalized at the maxima, the 370 nm band in the photoluminescence spectra is due to Raman scattering.

the QDs had no absorption (Fig. 2b, spectrum 2). Such differentiation was also observed in the HNS PL excitation spectra.

The MC does not fluoresce at 440 nm, and thus the PL excitation spectrum of HNS-1 upon observation at 440 nm (Fig. 2b, 3) characterizes the QDs only and reproduces its absorption spectra. However, upon observation at the MC-FL emission maxima (520 nm), the PL excitation spectrum of HNS-1 contains both the MC-FL and QDs bands (Fig. 2b, 4) indicating the energy transfer from the QDs to the MC-FL.

The shoulder at 360 nm in the HNS PL extinction spectrum (Fig. 2b, spectrum 3) may be caused by the minor demethylation of the quaternized MC nitrogen during the HNS synthesis.²⁸ This effect was more pronounced in HNS-2 due to the significantly higher content of the MC-FL. In case of HNS-2, the 360 nm band was observed as a separate band and reproduced the absorption spectrum of styrylquinoline, the product of the MC-FL demethylation reaction.²⁹

The PL QYs of the free QDs and MC-FL are 0.0040 and 0.0076, respectively. The QDs QY in HNS-1 decreases to 0.0025, whereas the MC QY significantly increases up to 0.0160. In HNS-2 the QYs of the QDs and FL are 0.0020 and 0.0110, respectively. Thus, upon the QDs and the MC-FL binding in the HNS, the QY of the QDs decreases and that of the MC concomitantly increases due to the energy transfer from the former to the latter. As it was shown above, during the HNSs synthesis partial demethylation of MC may occur giving the styrylquinoline photochrome, which emits in the same spectral region as that of the QDs. The PL QY of the styrylquinoline photochrome is about 4 times greater than the QDs QY,³⁰ and thus the specified QYs of the QDs in the HNSs are the upper bounds.

Supposing the mechanism of energy transfer in this case being common for such systems, FRET, the distance between the QDs and MC was calculated⁶ to be 1.89 nm for HNS-1. The fact that the distribution of the HNSs of the different compositions is present in solution²⁵ was taken into consideration in the calculations. The calculation details can be found in the ESI.†

At this distance between the QDs and MC (1.89 nm), for HNS-2 (average $N = 5.6$) ϕ_{DA} should be 0.0007, which is less than the observed value of 0.0020. Apparently, the ϕ_{DA} overestimation was due to the demethylated FL, whose emission band overlaps with that of the QDs, as mentioned above.

The MC-FL is a structural analogue of the previously investigated styrylquinoline ligand.²⁹ The van der Waals size of the styrylquinoline *trans*-isomer in the maximal extended conformation along a long axis is 3.0 nm, whilst the sizes of the $(CH_2)_9$ chain and benzyl mercaptan are 1.0 nm.

The calculated $r = 1.89$ nm is the distance between the centers of the donor and acceptor. Since the QDs radius is 1.2 nm, the MC-chromophore (acceptor) is less than 0.7 nm from the QDs surface, *i.e.* it is incorporated into the benzyl mercaptan shell of the QDs. The assumed HNS structure, considering the size ratio of the QDs and ligands,²⁹ is shown in Scheme 1.

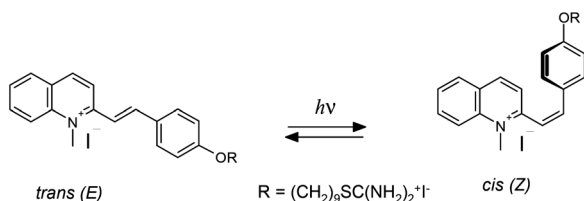
Thus, the flexible polymethylene chain is twisted in the HNS, and the MC-fragment is actually very close to the QDs surface. Apparently, the positively charged MC-fragment is adsorbed at the negatively charged sites on the QDs surface. This conclusion was confirmed by the photochemical properties of the HNSs, see below.

Photochemical properties

The MC-FL and HNSs contain the photoactive MC-group, which undergoes reversible *trans-cis* photoisomerization (Scheme 2).

Photolysis of the free MC-FL during the initial stage proceeds similarly to the photolysis of the other neutral and *N*-alkylated styrylquinoline derivatives.³⁰ Irradiation results in the changes in the spectral characteristic of photoisomerization: LWAB reduction and a hypsochromic shift in the absorption band maximum. The absorption kinetic curve reaches a plateau at the photostationary state (PS). The PS composition





Scheme 2 Photoisomerization of the MC-group in the FL.

and the spectrum of the *cis*-isomer were calculated using the Fischer method.³¹ However, a further slow LWAB decrease was observed upon an order of magnitude prolonged irradiation (see the inset in Fig. 4) testifying slow destruction of the FL. Therefore, the MC-FL forms a quasi-PS upon photolysis in DMF.

The absorption kinetics (*A*) upon reversible photoisomerization follows the differential eqn (1):³²

$$\frac{dA}{dt} = -(\varepsilon_t - \varepsilon_c) \cdot (\varphi_{tc} \cdot A_t - \varphi_{ct} \cdot A_c)(1 - 10^{-A}) \cdot I_0/A \quad (1)$$

where $A = A_t + A_c$, A_i and ε_i are an optical density and a molar extinction coefficient of isomer *i* (*trans* or *cis*) at the irradiation wavelength, φ_{tc} and φ_{ct} are the QYs of the *trans*–*cis* and *cis*–*trans* photoisomerization, and I_0 is the intensity of the applied light. An approximation by eqn (1) in the initial stage of the kinetic curve (until a PS) obtained by 462 nm light irradiation gives photoisomerization QYs of $\varphi_{tc} = 0.30$ and $\varphi_{ct} = 0.79$ (for the calculation method see ref. 32).

Eqn (2) was added to eqn (1) to take into account the FL photodestruction:³³

$$\frac{dA_i}{dt} = -\varepsilon_i \cdot A_i \cdot \varphi_d \cdot (1 - 10^{-A}) \cdot I_0/A, \quad (2)$$

where φ_d is the QY of the FL photodestruction, which presumably does not depend on the FL isomer form (see discussion below, the principal component analysis shows that both the *trans*- and *cis*-FL undergo photodestruction). Joint numerical integration of eqn (1) and (2) with the kinetics approximation in the full time range gives $\varphi_{tc} = 0.30$, $\varphi_{ct} = 0.82$ and $\varphi_d = 0.0017$. Thus, the photoisomerization QYs stays almost the same as in the “photoisomerization only” model and the photodestruction QY is two orders lower, allowing us to neglect the destruction during the early stages of photolysis. Considering that the MC-FL concentration was *ca.* 10^{-5} M, one can assume that the FL photodestruction (observed as the disappearance of the chromophore π -conjugated system) is caused by the minor impurities in DMF, which are absent in the solvents in which the MC-chromophore does not undergo photodestruction.³⁰

Photolysis of the HNSs was investigated upon irradiation at the LWAB region by 408 and 462 nm light. For instance, Fig. 3 shows the spectral changes observed upon irradiation of the HNS-2 by 462 nm light (Fig. 3a) and 408 nm light (Fig. 3b).

A gradual and monotone decrease in the 420 nm LWAB was observed in both cases, but in the case of irradiation at

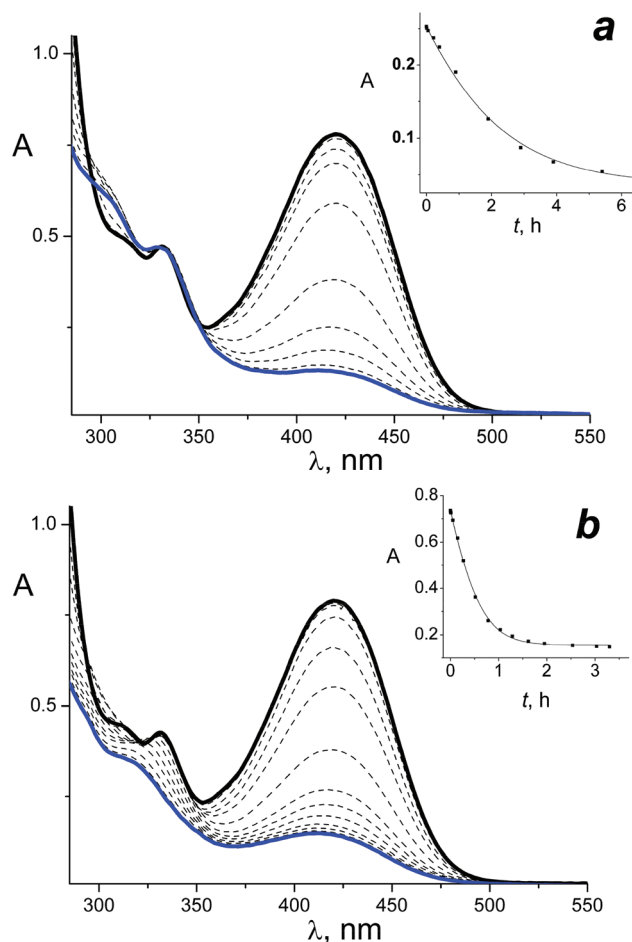


Fig. 3 The spectral changes upon HNS-2 irradiation (DMF) by (a) – 462 nm light (intensity 2.5×10^{-9} Einstein $\text{cm}^{-1} \text{s}^{-1}$), photolysis time 0, 30, 180, 780, 1440, 3240, 6840, 10 440, 14 040, 19 440 and 23 080 s; (b) – 408 nm light (intensity 7.8×10^{-9} Einstein $\text{cm}^{-1} \text{s}^{-1}$), photolysis time 0, 5, 30, 180, 540, 960, 1860, 2820, 3720, 4620, 5820, 7020, 9120, 10 920 and 11 880 s. Insets: The photolysis kinetics at the irradiation wavelengths and approximated curves (see text).

408 nm, it was accompanied by the short-wavelength absorption band decrease at 330 nm. Fig. 4 shows the kinetics of the absorbance changes at the absorption maxima of the QDs and MC, 330 nm and 420 nm, respectively. Similar spectral changes and difference between the 408 and 462 nm photolysis were observed upon HNS-1 irradiation.

Fig. 3 and 4 analysis leads to the following conclusions. A decrease in the LWAB upon HNS photolysis (Fig. 4, curves 1 and 3) is impossible to ascribe to the MC photoisomerization only because the absorption falls below the PS and even pure *cis*-MC level (Fig. 4, curve 5), which could be formed under the full photoisomerization of the *trans*-isomer (that is impossible due to the reaction reversibility). Thus, upon HNS irradiation at the MC-photochrome absorption band, the latter decomposes. In addition, the MC decomposition products are colored (the absorption does not fall to zero), but they have significantly lower extinction coefficients than the initial *trans*-MC.



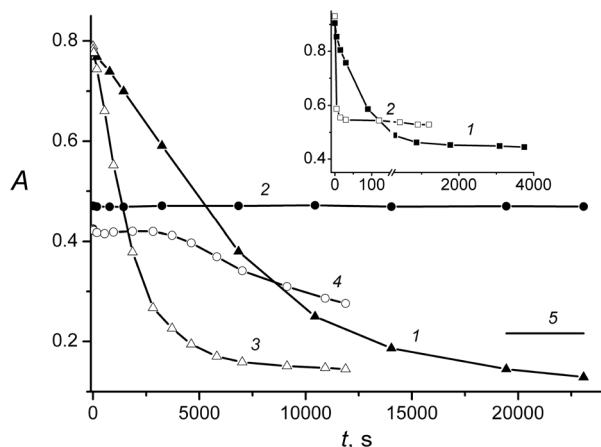


Fig. 4 The absorption kinetics at 420 nm (1, 3) and 330 nm (2, 4) upon HNS-2 photolysis at 462 nm (1, 2) and 408 nm (3, 4); the absorption level of *cis*-MC-FL at the same concentration (5). Inset: The absorption kinetics at 420 nm upon free MC-FL photolysis at 462 nm (1) and 408 nm (2).

The QDs are quite stable upon the HNSs irradiation by 462 nm light (Fig. 3a and 4, curve 2), and the absence of absorption changes testifies that the MC destruction products have a 330 nm absorption equal to the initial *trans*-isomer. However, upon HNSs photolysis by light of a higher energy (408 nm), the intensity reduction, widening and hypsochromic shift of the QDs absorption band were observed (Fig. 3b). Similar spectral changes were observed previously in the case of QDs irradiation in the region of its absorbance – by the 316 nm and 370 nm light – and were explained by the QDs photodestruction.²⁷

However, the QDs studied do not absorb visible light, and the model experiment showed that the free QDs do not undergo any changes under 408 and 462 nm irradiation (with the same irradiation times). Hence, under HNSs irradiation by 408 nm light, a sensitized photodestruction of the QDs takes place. In addition, as the comparison of curves 3 and 4 in Fig. 4 shows, this process starts only at the quite late stage of the MC-FL photolysis and may be caused by the accumulation of the MC photodestruction products.

Application of principal component analysis (PCA) can give additional information about the photoreactions that the HNS undergo.^{34,35} The scores plots are shown in Fig. 5, where the experimental spectra are represented on the basis of the first two singular vectors. Each point in the plot corresponds to the specific spectra upon photolysis. Two spectral ranges were considered, where both components of the HNSs absorb (300–510 nm, Fig. 5) and where only MC absorbs (420–510 nm, Fig. 5, inset). The spectra were recorded with 1 nm steps. Spectral changes upon the free MC-FL photolysis were added to the analyzed matrix for the comparison.

Plot 1 in Fig. 5 characterizes the spectral changes upon HNS-2 irradiation by 462 nm light. As shown above, these changes were caused by the MC-FL transformations. The linearity of the PCA plot indicates that only the two chromophores

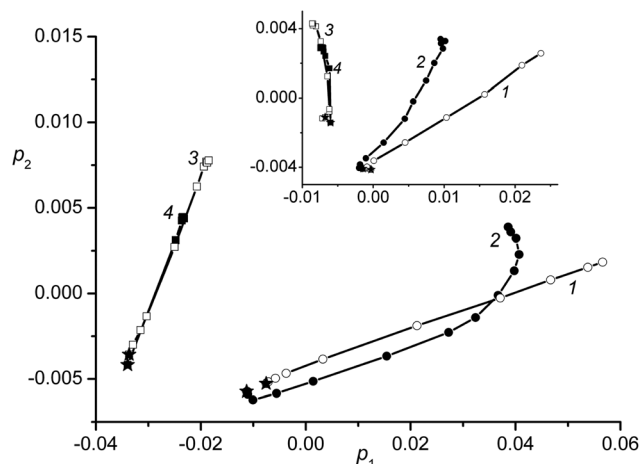


Fig. 5 Principal component analysis of the spectral changes (scores plots) in the range of 300–510 nm, which take place upon photolysis of HNS-2 (1, 2) and the MC-FL (3, 4) by 462 nm light (1, 3) and 408 nm light (2, 4); the experimental spectra are represented on the basis of the first two singular vectors p_1 and p_2 . The first spectra of each series are marked by asterisks. Inset: The same analysis for the 420–510 nm spectral range (see text).

are present in the reaction mixture. In this case, the chromophores are HNS with *trans*-MC and HNS with the MC photolysis products.

The absence of the third chromophore (HNS with *cis*-MC-FL) testifies that the MC photoisomerization was blocked in the HNS. This conclusion was confirmed by the PCA of the HNS LWAB where only the MC absorbs (Fig. 5, inset, plot 1). The absence of plot deviations along the third singular vector coordinate confirms that only the two chromophores are present in the reaction mixture. The photoisomerization blocking was associated with the MC-group (within the benzyl mercaptan shell) proximity to the QDs surface (up to adsorption on the surface), which creates steric constraints for the reaction.

The initial spectral changes upon HNS irradiation by 408 nm light (Fig. 5, plot 2) are similar to those observed under 462 nm irradiation (plot 2 is parallel to the plot 1). However, plot 2 then deviates testifying that the additional chromophores are formed in the reaction mixture. The bending point of the plot 2 (Fig. 5, the 7th spectrum in the series) corresponds to the beginning of the QDs absorbance decrease (Fig. 4, curve 4), *i.e.* the start of the additional chromophores formation correlates with the start of the QDs destruction and may be ascribed to this process. Plots 3 and 4 (Fig. 5) show the free MC-FL photolysis PCA in joint basis are linear and characterize the photoisomerization of the two chromophores only (*trans*- and *cis*-MC). Minor spectral changes caused by the MC-FL photodestruction are negligible against the significant changes in the MC photoisomerization and HNS photodestruction. However, the MC-FL photodestruction was noticeable upon the separate analysis of the MC absorbance band (Fig. 5, inset). Plots 3 and 4 in the inset are



arc-like curves and testify that simultaneous photoisomerization and photodestruction takes place and at least three chromophores were involved.

Comparative analysis of the MC absorption band only (Fig. 5, inset) reveals two more features. First, the initial points of the plots (marked by asterisks) corresponding to the *trans*-MC in HNS (plots 1 and 2) and the free form (plots 3 and 4) are different, *i.e.* the MC LWAB changes upon FL incorporation to the HNS. This fact shows the interaction between the MC-chromophore and QDs, and is in accordance with the assumption (see above) that the MC-fragment of the FL is adsorbed on the QDs surface (due to the spacer flexibility) and forms states such as surface charge transfer complexes leading to the LWAB shape change. The second feature of plots 1 and 2 (Fig. 5, inset) is their different direction revealing that the products of MC photodestruction by 408 and 462 nm light have different absorption spectra. This may be caused by the formation of different products under photolysis of MC in the HNS by 408 and 462 nm light in contradistinction to the free MC-FL photolysis for which plots 3 and 4 (Fig. 5, inset) match each other.

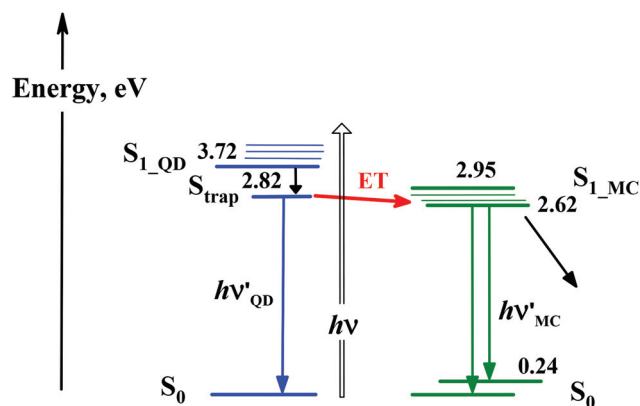
However, there is another possible explanation for this feature. The products of the MC-photodestruction could be the same, but in the case of irradiation by 462 nm light they are adsorbed on the QDs surface, whilst upon 408 nm light irradiation they gradually desorb due to the destruction of the QDs and transfer to the solution. Deviation of plot 2 (Fig. 5, inset) to the direction of plots 3 and 4 (which characterize the reactions of free MC-FL) supports this hypothesis.

The spectral changes observed upon HNS-1 photolysis by 408 and 462 nm light do not differ from the case of HNS-2, so their analysis leads to the very same conclusions.

Since the MC photoisomerization in the HNS is blocked, the experimental kinetics of the HNS photolysis was fitted by eqn (2); examples of the calculated kinetics are shown in the insets in Fig. 3. The photodestruction QY of the MC in HNS is 0.0040 (for 462 nm irradiation).

Thus, a comparison of the photolysis of the MC-FL in the free form and incorporated to the HNS shows that the attaching the QDs surface leads to the FL photoisomerization suppression and photodestruction acceleration. Photodestruction of the QDs takes place upon HNS photolysis by light with an energy higher than the threshold, presumably due to the electron transfer from the QDs to the MC since the cation of latter is an electron acceptor. TD B3LYP/6-31G* calculations³⁶ show that the LWAB of the MC-FL in the visible region characterizes only the S_1 excited state and corresponds to the electron transfer from the highest occupied molecular orbital to the lowest unoccupied orbital. The higher energy states (S_n), which may participate in the oxidation of the QDs, are not excited upon irradiation in the LWAB range.

To explain the observed effects we suggest considering the electronic states diagram of the HNS (Scheme 3). The MC-FL absorption band maximum (420 nm) corresponds to an energy of 2.95 eV. The excited vibrational levels of the S_1 -state are populated upon irradiation at the band maximum. The $S_0 \rightarrow$



Scheme 3 The electronic states diagram of the HNS. The levels of the ground (S_0) and lowest excited (S_1) states of the QDs and MC-FL, and the level of the QDs surface trap are shown. The processes corresponding to the light absorption ($h\nu$) and emission ($h\nu'$), ET and the FL photochemical reaction are also shown.

S_1 0–0 transition of MC (cross point of the absorption and emission spectra) has an energy of 2.62 eV. The FL fluorescence maximum corresponds to an energy of 2.38 eV and emission of light with this energy leads to the population of the excited vibrational levels of the S_0 -state with an energy of 0.24 eV. In addition, the photophysical processes, photochemical reactions take place upon MC-FL excitation to the S_1 -state.

The QD absorption maximum (333 nm) corresponds to a band gap of 3.72 eV. The fluorescence of the investigated QDs has a trap states origin²⁵ and the emission maximum (440 nm) corresponds to an energy of 2.82 eV. Low intensive direct transitions $S_0 \rightarrow S_{\text{trap}}$ are not noticeable against the intensive QDs band gap absorption and upon free QDs irradiation, the S_{trap} states are populated through the S_{1_QD} state (Scheme 3). Apparently, in addition to the trap-state emission, the S_{trap} state population leads to the slow QDs degradation under UV irradiation.²⁷

Upon HNS irradiation with visible light at the LWAB range, the S_{trap} HNS may be populated through the S_{1_MC} state of the adsorbed MC-FL (*i.e.* through surface charge transfer complexes). The energy of the light with wavelengths of 408 and 462 nm is 3.04 and 2.68 eV, respectively. Thus, the light quantum has enough energy for the S_{trap} state population in the first case only explaining a peculiar “threshold effect” – the different behavior of the HNS upon irradiation with visible light at different wavelengths. Investigation of the photolysis kinetics shows that the MC-FL photodestruction products adsorbed on the QDs surface may be the sensitizers of the QDs photodegradation.

Experimental

The HNSs were synthesized *via* a one-pot, non-injective, microwave assisted technique. The details can be found elsewhere.^{25,26} The electronic absorption and emission spectra



were recorded on a UV-VIS spectrometer Specord M-400 and PerkinElmer LS 55 Fluorescence spectrometer, respectively. The fluorescence QYs were measured using a dilute alcoholic solution of either anthracene (fluorescence QY 0.3 (ref. 37)) or 1-(9-anthryl)-2-(2-quinolyl)ethylene (fluorescence QY 0.03 (ref. 38)) as the reference, and the measuring accuracy was 10%.

The absorption of the solutions for the PL measurements did not exceed 0.1. Arrays of light emitting diodes were applied for UV irradiation – LED-408 (BL L513-UV, $\lambda_{\text{max}} = 408$ nm, FWHM = 15 nm) and LED-462 (SDK 470-45-3/2, $\lambda_{\text{max}} = 462$ nm, FWHM = 20 nm). The light intensities were $(2.4\text{--}7.8) \times 10^{-9}$ Einstein $\text{cm}^{-2} \text{s}^{-1}$ for LED-408 and $(1.6\text{--}2.5) \times 10^{-9}$ Einstein $\text{cm}^{-2} \text{s}^{-1}$ for LED-462 (actinometry was carried out with ferric oxalate). The measuring accuracy of the photoisomerization QY was 20%.

Conclusions

Investigation of the photochemical properties of HNSs containing CdS QDs and photochromic MC-FL shows the fluorescence quenching of the first and sensitization of the latter due to the ET from the QDs to the MC. In the HNS, the MC-group of FL is presumably adsorbed at the QDs surface, as indicated by the small distance between the MC and QDs calculated from the QDs fluorescence decrease as a result of the ET to the MC, by deformation of the MC absorption band in the HNS when compared to the free MC-FL and by the restriction of the MC *trans*-*cis*-photoisomerization in the HNS due to steric constraints. Besides, the MC photoisomerization restriction, the MC photodestruction is accelerated in the HNS. Upon HNS photolysis by visible light with an energy higher than the threshold, the photosensitized destruction of the QDs (which does not absorb the applied light) takes place, presumably due to the surface electron trap states of the QDs population with participation of the MC photodestruction products adsorbed on the QDs surface. In the case of irradiation by light with energy that is not sufficient for the surface trap states population, the QDs are stable and the MC only undergoes photodestruction.

Acknowledgements

The authors are grateful to S. B. Brichkin for the valuable discussion.

Notes and references

- 1 A. Credi, *New J. Chem.*, 2012, **36**, 1925.
- 2 S. Silvi and A. Credi, *Chem. Soc. Rev.*, 2015, **44**, 4275.
- 3 R. Klajn, J. F. Stoddart and B. A. Grzybowski, *Chem. Soc. Rev.*, 2010, **39**, 2203.
- 4 R. Freeman and I. Willner, *Chem. Soc. Rev.*, 2012, **41**, 4067.
- 5 T. Avellini, C. Lincheneau, F. Vera, S. Silvi and A. Credi, *Coord. Chem. Rev.*, 2014, **263**–**264**, 151.
- 6 L. Medintz and H. Mattoussi, *Phys. Chem. Chem. Phys.*, 2009, **11**, 17.
- 7 C. Mongin, S. Garakyaraghi, N. Razgoniaeva, M. Zamkov and F. N. Castellano, *Science*, 2016, **80**, 369–371.
- 8 K. V. Vokhmintcev, P. S. Samokhvalov and I. Nabiev, *Nano Today*, 2016, **11**, 189–211.
- 9 I. L. Medintz, S. A. Trammell, H. Mattoussi and J. M. Mauro, *J. Am. Chem. Soc.*, 2004, **126**, 30.
- 10 L. Zhu, M. Zhu, J. K. Hurst and A. D. Q. Li, *J. Am. Chem. Soc.*, 2005, **127**, 8968.
- 11 Z. Erno, I. Yildiz, B. Gorodetsky, F. M. Raymo and N. R. Branda, *Photochem. Photobiol. Sci.*, 2010, **9**, 249.
- 12 S. A. Diaz, G. O. Menendez, M. H. Etchelon, L. Giordano, T. M. Jovin and E. A. Jares-Erijman, *ACS Nano*, 2011, **5**, 2795.
- 13 W. R. Algar, H. Kim, I. L. Medintz and N. Hildebrandt, *Coord. Chem. Rev.*, 2014, **263**–**264**, 65.
- 14 S. A. Diaz, F. Gillanders, E. A. Jares-Erijman and T. M. Jovin, *Nat. Commun.*, 2015, **6**, 6036.
- 15 S. A. Diaz, L. Giordano, T. M. Jovin and E. A. Jares-Erijman, *Nano Lett.*, 2012, **12**, 3537–3544.
- 16 M. H. Stewart, A. L. Huston, A. M. Scott, E. Oh, W. R. Algar, J. R. Deschamps, K. Susumu, V. Jain, D. E. Prasuhn, J. Blanco-Canosa, P. E. Dawson and I. L. Medintz, *ACS Nano*, 2013, 9489–9505.
- 17 A. Boulesbaa, Z. Huang, D. Wu and T. Lian, *J. Phys. Chem. C*, 2010, **114**, 962–969.
- 18 M. D. Rao and G. Pennathur, *Mater. Res. Bull.*, 2017, **85**, 64.
- 19 J. Mao, X. M. Chen and X. W. Du, *J. Alloys Compd.*, 2016, **656**, 972.
- 20 J. Zhang, Y. Guo, H. Fang, W. Jia, H. Li, L. Yang and R. Wang, *New J. Chem.*, 2015, **39**, 6951.
- 21 M. F. Budyka and V. M. Li, *ChemPhysChem*, 2017, **18**, 260.
- 22 M. F. Budyka, N. I. Potashova, T. N. Gavrishova and V. M. Li, *Nanotechnol. Russ.*, 2012, **7**, 280.
- 23 M. Majumder, S. Karan and B. Mallik, *J. Lumin.*, 2011, **131**, 2792.
- 24 M. F. Budyka, O. V. Chaschikhin and P. A. Nikulin, *Nanotechnol. Russ.*, 2015, **10**, 13.
- 25 M. F. Budyka, O. V. Chaschikhin and P. A. Nikulin, *Nanotechnol. Russ.*, 2016, **11**, 78.
- 26 O. V. Chashchikhin, M. F. Budyka, T. N. Gavrishova and V. M. Li, *RSC Adv.*, 2017, **7**, 2236.
- 27 M. F. Budyka and O. V. Chaschikhin, *High Energy Chem.*, 2016, **50**, 349.
- 28 D. Aumann and L. W. Deady, *J. Chem. Soc., Chem. Commun.*, 1973, **2**, 32.
- 29 M. F. Budyka, O. V. Chashchikhin, T. N. Gavrishova, M. G. Spirin and S. B. Brichkin, *Nanotechnol. Russ.*, 2014, **9**, 116.
- 30 M. F. Budyka, V. M. Li and T. N. Gavrishova, *High Energy Chem.*, 2014, **48**, 376.



- 31 R. Gade and T. Porada, *J. Photochem. Photobiol., A*, 1997, **107**, 27.
- 32 M. F. Budyka, N. I. Potashova, T. N. Gavrishova and V. M. Li, *High Energy Chem.*, 2008, **42**, 446.
- 33 M. F. Budyka, V. M. Li, T. N. Gavrishova and N. I. Potashova, *High Energy Chem.*, 2015, **49**, 158.
- 34 A. L. Pomerantsev, *Chemometrics in Excel*, John Wiley & Sons, Inc., Hoboken, 2014.
- 35 Y. B. Monakhova and I. Yu. Goryacheva, *TrAC, Trends Anal. Chem.*, 2016, **82**, 164–174.
- 36 M. J. Frisch, G. W. Trucks, H. B. Schlegel, *et al.*, *Gaussian 09, Revision B.01*, Gaussian, Inc., Wallingford CT, 2010.
- 37 H. D. Becker, *Chem. Rev.*, 1993, **93**, 145.
- 38 M. F. Budyka, N. I. Potashova, T. N. Gavrishova and V. M. Li, *High Energy Chem.*, 2014, **48**, 185.

